Robotica (2007) volume 25, pp. 297–305. © 2006 Cambridge University Press
doi:10.1017/S0263574706003092 Printed in the United Kingdom

Contour tracking of an unknown planar object by regulating force for mobile robot navigation

Seul Jung[†]*, Poongwoo Jeon[†] and T. C. Hsia[‡]

[†]*BK 21 Mechatronics Group, Intelligent Systems and Emotional Engineering Laboratory, Chungnam National University, Daejeon 305-764, Korea*
[‡]*Department of Electrical and Computer Engineering, University of California, Davis, CA 95616, USA*

(Received in Final Form: August 18, 2006. First published online: September 7, 2006)

SUMMARY
In this paper, a novel contour-tracking control method of an unknown planar object by lateral force regulation for wheeled mobile robot navigation is presented. The robot is required to follow the contour of an unknown object toward the goal position. Based on mobile robot dynamic equations, a force-control algorithm is proposed to maintain constant contact with a planar object. Measured contact force from an object is used not only to regulate a contact force in a lateral direction, but also to control the orientation angle of the robot to avoid collision with an object. Simulation and experiment of contour-tracking tasks of a wheeled mobile robot are conducted. Experimental results show that the contact force is well-regulated, and the robot arrives at the goal position successfully.

KEYWORDS: Contour tracking; Mobile robot navigation; Force control.

1. Introduction

Nowadays, mobile robot is in a great demand in robotics research due to its ability to move to any place in its terrain. Transition from robots in a fixed frame to robots in a moving frame brings them closer to our living environment. The mobility of the robot makes many applications possible. A variety of tasks depend on mobility such as exploration on Mars, outdoor investigations, search-and-rescue jobs in hazardous areas, carrying and handling services inside buildings, and working in cooperation with humans/robots. Successful mobility requires three core techniques: localization, path planning, and control. These core techniques are necessary in most of the mobile robot applications.

On the basis of workspaces, mobile robot applications can be divided into three domains. The first domain is a self-domain where robots move freely. Required techniques for self-domain include autonomous navigation and collision avoidance to conduct given tasks at the specific location.[1–5] For successful autonomous navigation and control, robots should overcome dead-reckoned situation with suitable sensor fusion algorithms with local and global sensors. In a control aspect, extensive research on position control of a mobile robot has been carried out.[6–12] The second domain of interest in mobile robot research is called a cooperative working domain where the robot interacts with robots, humans, or objects. Soccer robot game is a good example of a cooperative working domain. The last domain is the constrained domain in which robots are not allowed to move freely, but they remain constrained by the environment. Relatively, researches on robots in the constrained domain have not been carried out actively because of a lack of demand from industries or individuals. However, research on cooperative working robots in the constrained environment has received greater attraction recently. Robots are required to interact more with humans or other robots to perform cooperative tasks in the constrained domain.

In this constrained framework, interaction of the mobile robot with an object forms the basis of not only position control but also sophisticated force control. The mobile robot should perform two control operations simultaneously: one is to follow the contour of a planar object and the other is to regulate the interaction force. To do that, a force-control algorithm is used. Force control has been mainly used for constrained robot manipulators to cope with interactive force from counterparts.[13–18]

Here, we propose a novel concept of contour-tracking algorithm of an unknown object based on a force-control method for a nonholonomic wheeled-drive mobile robot (WMR). The WMR is required to follow the contour of an unknown planar object with a constant desired force. To the best of our knowledge, a research of this kind has not been carried out so far. Similarity can be found in lateral position control of autonomous highway vehicles.[19–21]

The force-control law is formed from an explicit force error that is defined as the difference between a desired force and an applied normal force. The explicit force-control method is similar to the hybrid force control, which is one of the two well-known force-control algorithms in the literature: impedance force control and hybrid force control.[13,14] Modified versions of the two force-control algorithms have also been proposed.[15–17] Here, the explicit force-control algorithm is used for contour tracking of a mobile robot. Simulation studies are performed based on dynamics models to confirm the proposed algorithm. Furthermore, experimental studies are also conducted to show that the mobile robot successfully follows the arbitrary contour of the environment by regulating a desired force.

*Corresponding author. E-mail: jungs@cnu.ac.kr

https://doi.org/10.1017/S0263574706003092 Published online by Cambridge University Press

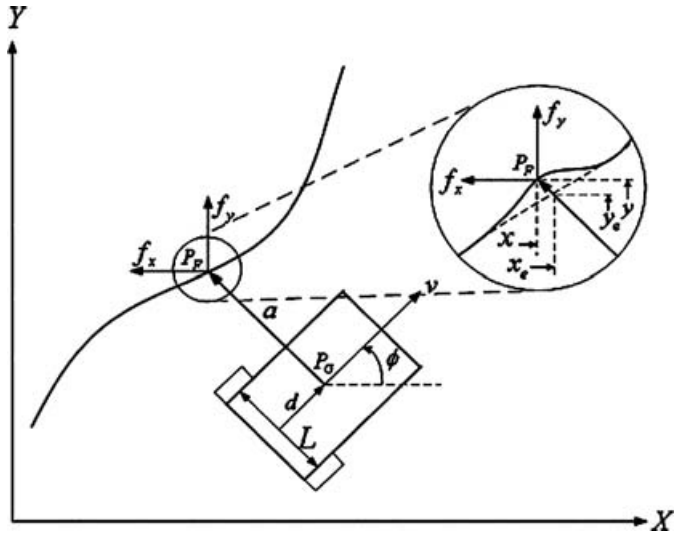


Fig. 1. Kinematics of the mobile robot.

2. Mobile Robot Kinematics

Many control applications of the mobile robot are based on the kinematics model. Figure 1 shows the coordinate relationship between the mobile robot and the object. v is the linear velocity and ω is the angular velocity of the mobile robot at the contact point P_f. The mobile robot kinematics is given by

$$\begin{bmatrix} \dot{x} \\ \dot{y} \\ \dot{\phi} \end{bmatrix} = \begin{bmatrix} \cos\phi & -d\ \sin\phi - a\ \cos\phi \\ \sin\phi & d\ \cos\phi - a\ \sin\phi \\ 0 & 1 \end{bmatrix} \begin{bmatrix} v \\ \omega \end{bmatrix} \tag{1}$$

where x and y are the robot positions, ϕ is the heading angle of the robot in the global coordinates, d is the distance between the center of gravity P_G and the center of the wheel axis, and a is the distance between the center of gravity and the force sensor. The velocities of the mobile robot can be represented by the relationship between the joint space and the Cartesian space as

$$\begin{bmatrix} v \\ \omega \end{bmatrix} = \begin{bmatrix} r/2 & r/2 \\ r/L & -r/L \end{bmatrix} \begin{bmatrix} \dot{\theta}_R \\ \dot{\theta}_L \end{bmatrix} \tag{2}$$

where r is the radius of the wheel, L is the distance between the two wheels, and $\dot{\theta}_R$ and $\dot{\theta}_L$ are the velocities of the right and the left wheels, respectively. From Eqs. (1) and (2), the following Jacobian relationship can be obtained:

$$\dot{X} = J\dot{\theta} \tag{3}$$

where $\dot{X} = \begin{bmatrix} \dot{x} & \dot{y} & \dot{\phi} \end{bmatrix}^T$, $J = \begin{bmatrix} j_{11} & j_{12} \\ j_{21} & j_{22} \\ j_{31} & j_{32} \end{bmatrix}$, $\dot{\theta} = \begin{bmatrix} \dot{\theta}_R & \dot{\theta}_L \end{bmatrix}^T$,

and each element of the Jacobian J is given as

$$j_{11} = \frac{r}{2}\cos\phi - \frac{r}{L}(d\ \sin\phi + a\ \cos\phi)$$

$$j_{12} = \frac{r}{2}\cos\phi + \frac{r}{L}(d\ \sin\phi + a\ \cos\phi)$$

$$j_{21} = \frac{r}{2}\sin\phi + \frac{r}{L}(d\ \cos\phi - a\ \sin\phi)$$

$$j_{22} = \frac{r}{2}\sin\phi - \frac{r}{L}(d\ \cos\phi - a\ \sin\phi),$$

$$j_{31} = \frac{r}{L}$$

$$j_{32} = -\frac{r}{L}.$$

Since the mobile robot is a nonholonomic system, the Jacobian matrix is not a square.

3. Mobile Robot Dynamics

Generally, since the mobile robot is moving on the plane, the dynamics of the mobile robot depends on kinetic rather than potential energy. Then, the mobile robot dynamic equation can be formed as in ref. 6.

$$M(q)\ddot{q} + V(q, \dot{q}) = P(q)\tau - A^T\lambda \tag{4}$$

where $M(q)$ is the $n \times n$ inertia matrix, $V(q, \dot{q})$ is the $n \times 1$ Coriolis and centrifugal force, $P(q)$ is the $n \times m$ input transformation matrix, τ is the $m \times 1$ input torque vector, $A(q)$ is the $m \times n$ kinematics constraint matrix, and λ is a Lagrange's multiplier.

The kinematics constraint matrix $A(q)$ of pure rolling and no slipping conditions satisfies the equation as

$$A(q)\dot{q} = 0 \tag{5}$$

where $\dot{q} = [\dot{x}\ \dot{y}\ \dot{\phi}\ \dot{\theta}_R\ \dot{\theta}_L\ ]^T$.

Components of the mobile robot dynamic equation are given by

$$M(q) = \begin{bmatrix} m & 0 & -m_c d\sin\phi & 0 & 0 \\ 0 & m & m_c d\cos\phi & 0 & 0 \\ -m_c d\sin\phi & m_c d\cos\phi & I & 0 & 0 \\ 0 & 0 & 0 & I_W & 0 \\ 0 & 0 & 0 & 0 & I_W \end{bmatrix}$$

$$V(q, \dot{q}) = \begin{bmatrix} -m_c d\dot{\phi}^2\cos\phi \\ -m_c d\dot{\phi}^2\sin\phi \\ 0 \\ 0 \\ 0 \end{bmatrix}, \qquad P(q) = \begin{bmatrix} 0 & 0 \\ 0 & 0 \\ 0 & 0 \\ 1 & 0 \\ 0 & 1 \end{bmatrix},$$

$$A(q) = \begin{bmatrix} -\sin\phi & \cos\phi & -d & 0 & 0 \\ -\cos\phi & -\sin\phi & a & r/2 & r/2 \end{bmatrix}, \qquad \tau = \begin{bmatrix} \tau_R \\ \tau_L \end{bmatrix}$$

where m_c is the mass of the mobile robot without wheels, m is the total mass of the mobile robot, I is the moment about $\dot{\phi}$, and I_W is the moment of each wheel.

For simplicity, Lagrange's multiplier λ is eliminated.[6] To do that, the velocity vector of the mobile robot is given as

$$\dot{q} = S(q)\dot{\theta}(t) \tag{6}$$

where $\dot{\theta}(t) = [\dot{\theta}_R\ \dot{\theta}_L\ ]^T$. The matrix $S(q)$ is selected to satisfy the equation $S^T A^T \lambda = 0$.

https://doi.org/10.1017/S0263574706003092 Published online by Cambridge University Press

Substituting Eq. (6) into Eq. (5) yields

$$M(\dot{S}\dot{\theta} + S\ddot{\theta}) + V = P\tau - A^T\lambda. \tag{7}$$

Multiplying S^T to both sides of Eq. (7) and rearranging yields

$$S^T[M(\dot{S}\dot{\theta} + S\ddot{\theta}) + V] = S^T P\tau. \tag{8}$$

Since $S^T P\tau = \tau$, Eq. (8) becomes

$$S^T M S\ddot{\theta} + S^T M\dot{S}\dot{\theta} + S^T V = \tau. \tag{9}$$

The matrix S is selected to satisfy $S^T A^T\lambda = 0$ as

$$S(q) = \begin{bmatrix} r/2\,\cos\phi - r/L\,(d\sin\phi + a\cos\phi) & r/2\,\cos\phi + r/L\,(d\sin\phi + a\cos\phi) \\ r/2\,\sin\phi + r/L\,(d\cos\phi - a\sin\phi) & r/2\,\sin\phi - r/L\,(d\cos\phi - a\sin\phi) \\ r/L & -r/L \\ 1 & 0 \\ 0 & 1 \end{bmatrix} \tag{10}$$

where $b \equiv L/2$ and $c \equiv r/L$.

Substituting Eq. (10) into Eq. (9) yields the dynamics equation

$$\begin{bmatrix} D_{11} & D_{12} \\ D_{21} & D_{22} \end{bmatrix} \begin{bmatrix} \ddot{\theta}_{\mathrm{R}} \\ \ddot{\theta}_{\mathrm{L}} \end{bmatrix} + \begin{bmatrix} 2c^3bd\,(m + m_{\mathrm{c}})\left(\dot{\theta}_{\mathrm{R}}\dot{\theta}_{\mathrm{L}} - \dot{\theta}_{\mathrm{L}}^2\right) \\ 2c^3bd\,(m + m_{\mathrm{c}})\left(\dot{\theta}_{\mathrm{R}}\dot{\theta}_{\mathrm{L}} - \dot{\theta}_{\mathrm{R}}^2\right) \end{bmatrix} = \begin{bmatrix} \tau_{\mathrm{R}} \\ \tau_{\mathrm{L}} \end{bmatrix} \tag{11}$$

where

$$\begin{aligned} D_{11} &= c^2m\,[(b-a)^2 + d^2] + 2c^2d^2m_{\mathrm{c}} + c^2I + I_{\mathrm{W}} \\ D_{12} &= c^2\,[m\,(b^2 - a^2 - d^2) - 2d^2m_{\mathrm{c}} - I] \\ D_{21} &= c^2\,[m\,(b^2 - a^2 - d^2) - 2d^2m_{\mathrm{c}} - I] \\ D_{22} &= c^2m\,[(a+b)^2 + d^2] + 2c^2d^2m_{\mathrm{c}} + c^2I + I_{\mathrm{W}}. \end{aligned}$$

If we assume that the robot moves slowly on the plane, since in most of the cases it is true, then the Coriolis and centrifugal terms in Eq. (11) are assumed to be zero. Then, the dynamics equation is further simplified with the assumption of $d = 0$, which means that the center of gravity is located on the center of the wheel axis

$$\begin{bmatrix} D_{11} & D_{12} \\ D_{21} & D_{22} \end{bmatrix} \begin{bmatrix} \ddot{\theta}_{\mathrm{R}} \\ \ddot{\theta}_{\mathrm{L}} \end{bmatrix} = \begin{bmatrix} \tau_{\mathrm{R}} \\ \tau_{\mathrm{L}} \end{bmatrix}. \tag{12}$$

Therefore, the slowly moving mobile robot on the plane can be considered as a simple inertial system. This is the reason why most of the mobile robot control algorithms are satisfied with the kinematics model.

4. Force Control of the Mobile Robot

The dynamic equation of a force-controlled mobile robot from Eq. (12) can be defined as

$$D\ddot{\theta} = \tau - J^T h \tag{13}$$

where

$$\theta = \begin{bmatrix} \theta_{\mathrm{R}} \\ \theta_{\mathrm{L}} \end{bmatrix}, \qquad h = \begin{bmatrix} f \\ \mu \end{bmatrix}$$

f is the external force, μ is the external moment, and J is the Jacobian matrix as in Eq. (3).

The control law becomes

$$\tau = D\ddot{\theta} + J^T h. \tag{14}$$

From the Jacobian relationship between the joint space and the Cartesian space, we have the joint velocity

$$\dot{\theta} = J^{-1}\dot{X}. \tag{15}$$

We get the acceleration by differentiating Eq. (15)

$$\ddot{\theta} = J^{-1}(\ddot{X} - \dot{J}J^{-1}\dot{X}). \tag{16}$$

Since the Jacobian matrix is not invertible, the pseudo-inverse of the Jacobian is used as

$$\dot{\theta} = J^{*-1}\dot{X}. \tag{17}$$

Substituting the pseudo-inverse Jacobian into Eq. (16) yields

$$\ddot{\theta} = J^{*-1}(\ddot{X} - \dot{J}J^{*-1}\dot{X}) = (J^TJ)^{-1}J^T(\ddot{X} - \dot{J}(J^TJ)^{-1}J^T\dot{X}) \tag{18}$$

where $\dot{X} = [\dot{x}\ \ \dot{y}\ \ \dot{\phi}]^T$, $\dot{\theta} = [\dot{\theta}_{\mathrm{R}}\ \ \dot{\theta}_{\mathrm{L}}]^T$, and $J^{*-1} = (J^TJ)^{-1}J^T$.

We then define the output vector Y, which can be measured as

$$Y \equiv \begin{bmatrix} f_x & f_y & \phi \end{bmatrix}^T \tag{19}$$

where f_x and f_y are the contact forces on the x- and the y-axes, respectively.

As shown in Fig. 1, the contact force between the mobile robot and the object is modeled as

$$\begin{aligned} f_x &= k_{\mathrm{e}}\delta x \\ f_y &= k_{\mathrm{e}}\delta y \end{aligned} \tag{20}$$

where $\delta x = x - x_{\mathrm{e}}$, $\delta y = y - y_{\mathrm{e}}$, x_{e}, and y_{e} are the environment positions, x and y are the contact positions, and k_{e} is the stiffness of the environment object.

From Eq. (20), Y in Eq. (19) can be represented as

$$Y = K_{\mathrm{e}}\Delta X = K_{\mathrm{e}}(X - X_{\mathrm{e}}) = \begin{bmatrix} k_{\mathrm{e}} & 0 & 0 \\ 0 & k_{\mathrm{e}} & 0 \\ 0 & 0 & 1 \end{bmatrix} \begin{bmatrix} x - x_{\mathrm{e}} \\ y - y_{\mathrm{e}} \\ \phi \end{bmatrix}. \tag{21}$$

Since $\dot{X}_{\mathrm{e}} = 0$ and $\ddot{X}_{\mathrm{e}} = 0$ are assumed for unknown environments, Eq. (21) can be defined with $\dot{X}$ and $\ddot{X}$ as

$$\dot{X} = K_{\mathrm{e}}^{-1}\dot{Y}, \qquad \ddot{X} = K_{\mathrm{e}}^{-1}\ddot{Y}. \tag{22}$$

https://doi.org/10.1017/S0263574706003092 Published online by Cambridge University Press

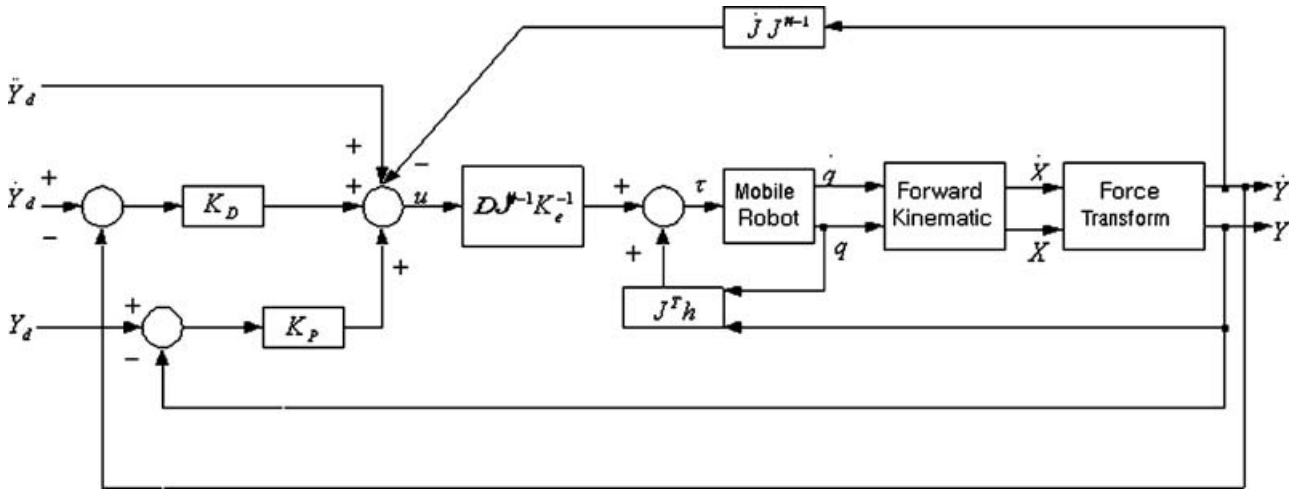


Fig. 2. Force control block diagram of the blind mobile robot as given in Eq. (25).

Substituting Eq. (22) into Eq. (18) yields

$$\ddot{\theta} = J^{*-1}(\ddot{X} - \dot{J}J^{*-1}\dot{X}) = J^{*-1}K_e^{-1}(\ddot{Y} - \dot{J}J^{*-1}\dot{Y}). \tag{23}$$

Substituting Eq. (23) into Eq. (14) yields the control law as

$$\tau = D\ddot{\theta} + J^T h = D\,[J^{*-1}K_e^{-1}(\ddot{Y} - \dot{J}J^{*-1}\dot{Y})] + J^T h. \tag{24}$$

Borrowing the concept of the explicit force-control method, the PD-type control input $\ddot{Y}$ is designed to minimize the force error directly as

$$\ddot{Y} = \ddot{Y}_d + K_D(\dot{Y}_d - \dot{Y}) + K_P(Y_d - Y) \tag{25}$$

where K_D and K_p are controller gains.

Substituting Eq. (25) into Eq. (24) yields the complete control law as

$$\begin{aligned}\tau = {} & DJ^{*-1}K_e^{-1}[\ddot{Y}_d + K_D(\dot{Y}_d - Y) \\ & - \dot{J}J^{*-1}\dot{Y} + K_P(Y_d - Y)] + J^T h\end{aligned} \tag{26}$$

where

$$D = \begin{bmatrix} D_{11} & D_{12} \\ D_{21} & D_{22} \end{bmatrix}, \qquad K_e = \begin{bmatrix} k_e & 0 & 0 \\ 0 & k_e & 0 \\ 0 & 0 & 1 \end{bmatrix},$$

$$K_D = \begin{bmatrix} k_{DX} & 0 & 0 \\ 0 & k_{DY} & 0 \\ 0 & 0 & k_{D\varphi} \end{bmatrix} x, \quad K_P = \begin{bmatrix} k_{PX} & 0 & 0 \\ 0 & k_{PY} & 0 \\ 0 & 0 & k_{P\varphi} \end{bmatrix}.$$

Combining Eq. (13) and Eq. (26) yields the ideal closed loop error equation as

$$\ddot{e} + K_D\dot{e} + K_P e = 0 \tag{27}$$

where $e = Y_d - Y$. So the force-tracking task can be achieved. Figure 2 shows the force-control block diagram of the mobile robot.

Note that the value of the environment stiffness K_e is required in the control law Eq. (26) to guarantee Eq. (27).

Table I. Simulation parameters.

Parameters	Value (cm)	Control parameters	Value
L	20	f_d	4 N
a	15	k_e	10,000 N/m
d	4	k_{px}, k_{py}	20,000
r	4	k_{dx}, k_{dy}	1,500

It is hard to measure environment stiffness and hence it is considered as an uncertainty. However, a close examination of Eq. (26) reveals that the value of environment stiffness is multiplied by a controller gain. This leads to the remark that the selection of controller gain affects the tracking performance without environment stiffness information.

5. Simulation Studies

For the simulation studies, robot parameters and control variables listed in Table I are used. For controller values, PD gains are set to large values. Since these values are divided by the stiffness k_e in Eq. (26), the actual values are relatively small. The environment is considered to be a soft object that has the stiffness of 10,000 N/m. The mobile robot is the nonholonomic system that has two control inputs ($\dot{\theta}_R$ and $\dot{\theta}_L$) and three outputs ($\dot{x}$, $\dot{y}$, and $\dot{\phi}$). The Cartesian values are obtained through forward kinematics to form the Cartesian errors. Figure 3 shows the straight contour-tracking result of the mobile robot. The corresponding heading angle and force-tracking plots are shown in Fig. 4. It is clear that the contact force is well-regulated at the desired value of 4 N after contact overshoot occurs.

6. Experimental Setup

The contact force is measured by a six-axis force sensor attached to the left of the robot, as shown in Fig. 5. The measured forces are decomposed into x- and y-directional forces, as shown in Fig. 1. The total force is a normal force to an object, which is calculated as the square root of the sum

https://doi.org/10.1017/S0263574706003092 Published online by Cambridge University Press

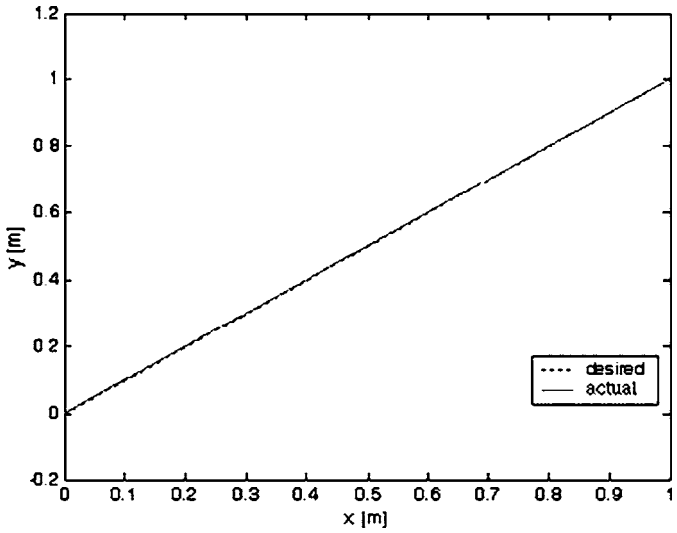


Fig. 3. Position tracking of the straight-line contour.

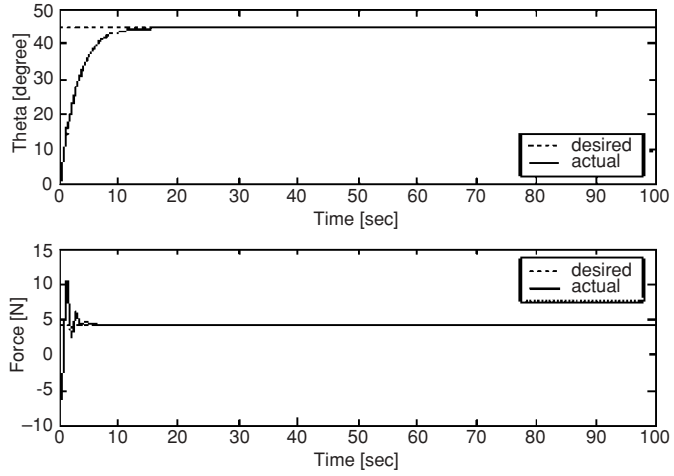


Fig. 4. Force and heading angle of the straight-line contour tracking shown in Fig. 2.

of x-directional force f_x and y-directional force f_y, as shown in the configuration of Fig. 1.

$$f_{\mathrm{e}} = \sqrt{f_x^2 + f_y^2}. \tag{28}$$

Two-axis force measurements f_x and f_y are used to calculate the orientation angle as

$$\phi = a\tan\left(\frac{f_y}{f_x}\right). \tag{29}$$

Therefore, if the robot maintains the same magnitude of force, then the orientation angle would be 45°. Hence, the desired orientation angle should be 45°. The orientation angle error e_ϕ is defined as the difference between a desired angle $\pi/4$ and a measured angle ϕ as

$$e_\phi = \frac{\pi}{4} - \phi. \tag{30}$$

The reason for defining the desired orientation angle to be $\pi/4$ is that the WMR should have a normal force direction to the object, as shown in Fig. 1. A force error is defined as

$$e_{\mathrm{f}} = f_{\mathrm{d}} - f_{\mathrm{e}} \tag{31}$$

where f_{d} is the desired force.

Here, the direction of the robot is controlled on the basis of force error measurements. Controlling the robot uses two measurement errors, a force directional error and a force magnitude error. For the sake of simplicity, since we do not know the exact dynamic model of the robot and the stiffness of the environment required in Eq. (26), the control input torque τ can be formed as a simple PD-type controller with objectives of minimizing a force error and an orientation angle error. Note that the controller gains for the right and the left wheel have opposite sign configurations to make turns.



Fig. 5. Experimental setup.

https://doi.org/10.1017/S0263574706003092 Published online by Cambridge University Press

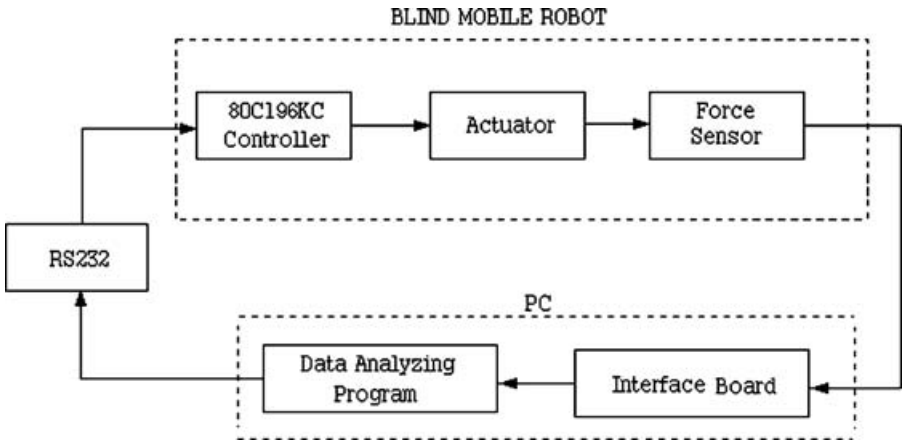


Fig. 6. Control block diagram of the robot.

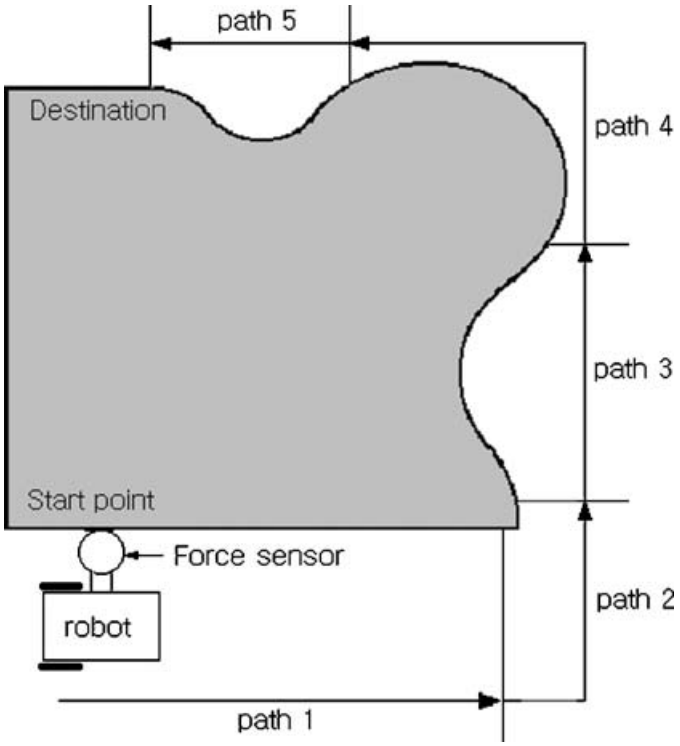


Fig. 7. Environmental contour.

The experimental setup is shown in Fig. 5. The whole system consists of a mobile robot with a force sensor, an interface program for control algorithms in a PC, and a communication module. The mobile robot with a force sensor moves the arbitrary contour. The sensed force data are transferred to a PC through serial communication, and processed to obtain the heading angle of the robot. The overall block diagram is shown in Fig. 6. The arbitrary contour is made of wood with the shape shown in Fig. 7. It has three different contours: straight line, concave, and convex. The robot is required to follow this unknown contour of a planar object by regulating a desired force.

The direction and orientation of the robot are determined by the speed of each wheel. The robot is commanded to follow the contour of the environment while maintaining contact with it. The JR3 force sensor is mounted on a robot to detect forces in the x- and y-directions. To minimize the frictional force, a bearing is attached to the force sensor. Hence, the normal force is considered in all our experiments. Only two forces, the x- and y-directional ones are used in the control algorithm developed in a PC to generate the command signal for each wheel. The command signals are sent by serial communication between the robot and the PC.

7. Experimental Results

The robot is tested to follow the wall shown in Fig. 7. The desired force is set to 4 N and the desired orientation angle is set to 45°. Depending on the contours, the controller gains for the right and the left wheels are selected having different signs or magnitudes. Specially, for the concave contour shown in Fig. 7, the controller gains should be selected with care. For example, the left wheel moves forward, but the right-sided wheel should move backward to get out of the deep concave contour.

First, the robot is commanded to follow each contour separately. The traveling time is 4 s. Figure 8 shows the tracking results for a straight-line contour. The heading angle approximately has a 4° offset error because the robot tries to maintain contact by pushing against the wall. This is clearly shown in the force plot of Fig. 8. Contact force is well maintained at a desired level.

Next, the robot is tested with respect to a concave contour. As shown in Fig. 9, an average of heading angle errors is almost zero and the contact force is well maintained at a desired level. Figure 10 shows the tracking results for a convex contour. The robot successfully follows the contour without losing contact. The contact force is well regulated and a heading angle error is almost zero.

Finally, the robot is tested for a whole contour-tracking task. The whole traveling time taken is about 50 s. The controller gains are fixed for the whole contour-tracking task. The results are shown in Fig. 11. The heading angle error suddenly rises to 45° in 8 s and the force drops to near zero. This means that the robot moves along path 2 of Fig. 7 and it loses contact with the wall because the shape

https://doi.org/10.1017/S0263574706003092 Published online by Cambridge University Press

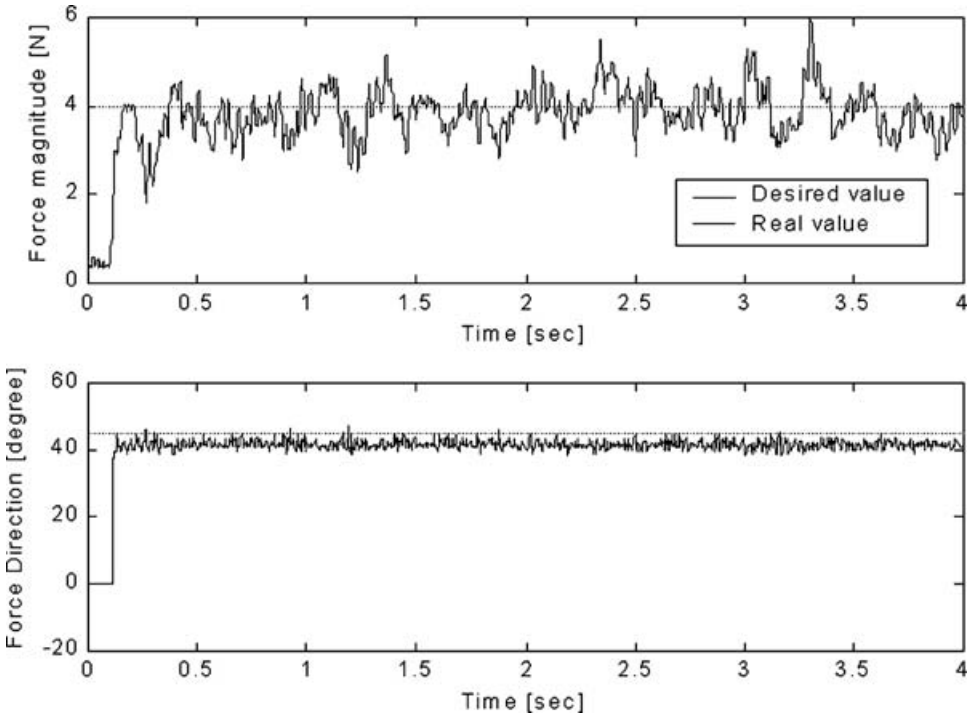


Fig. 8. Tracking result of path 1, which is a straight-line contour.

of the wall has a sharp edge. Hence, the robot slowly turns its heading direction and follows the concave contour. At around 23 and 45 s, the force plot shows large overshoots. This is the time when the robot passes the concave shape. The reason why the second overshoot at 45 s is larger than the first one is because the radius of the second concave shape is smaller than that of the first one. A tracking control task is more difficult when the radius of the concave contour is small.

8. Conclusion

In this paper, the force-control application of a wheeled mobile robot for an unknown contour of a planar object is presented. The force-control algorithm is derived on the basis

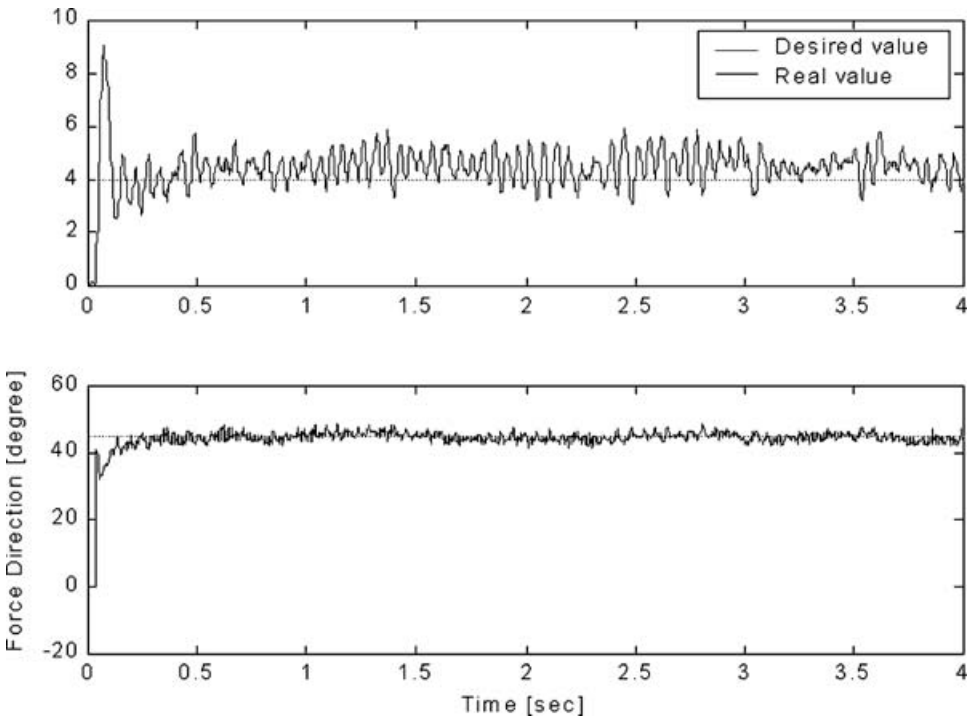


Fig. 9. Tracking result of a concave contour.

https://doi.org/10.1017/S0263574706003092 Published online by Cambridge University Press

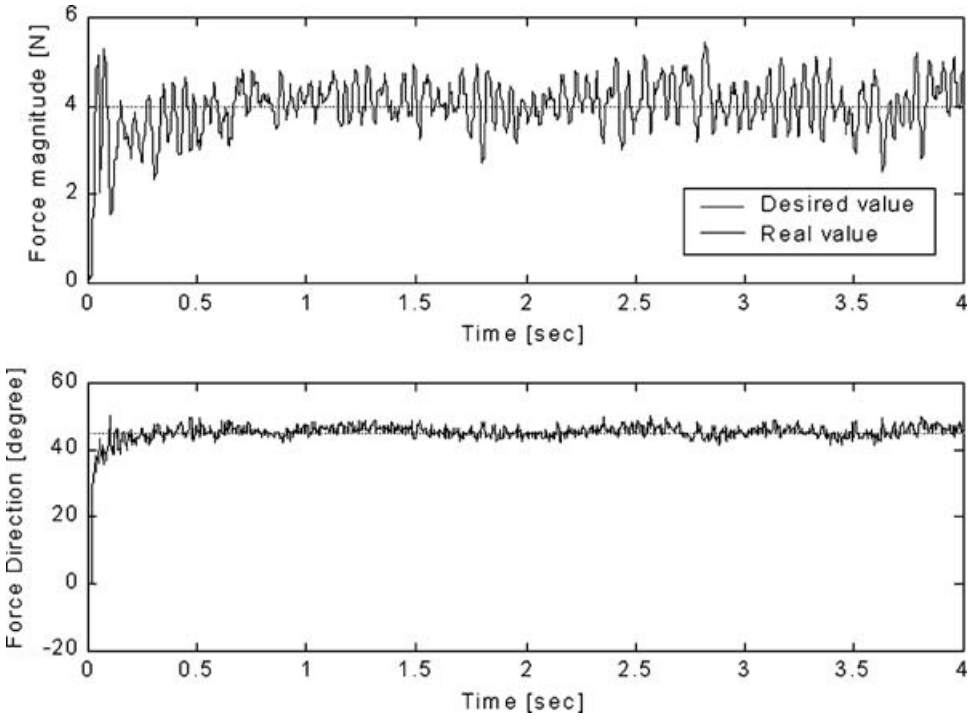


Fig. 10. Tracking result of a convex contour.

of a mobile robot dynamics model. Simulation results show a good tracking performance. The WMR successfully moves toward the goal position while regulating a desired force. Experimental studies show good force-tracking results of the robot for various shapes of the environment.

The proposed idea can be used for force-control application of robots that require contact with objects such as welding robots in the ship-building industry. To save cost of the workers, the mobile robot can be replaced to perform jobs such as painting or welding. These tasks require sophisticated force-control algorithms. Another application could be a collision-avoidance technique by using force field regulated by the proposed force-control algorithm. This is an ongoing research topic.

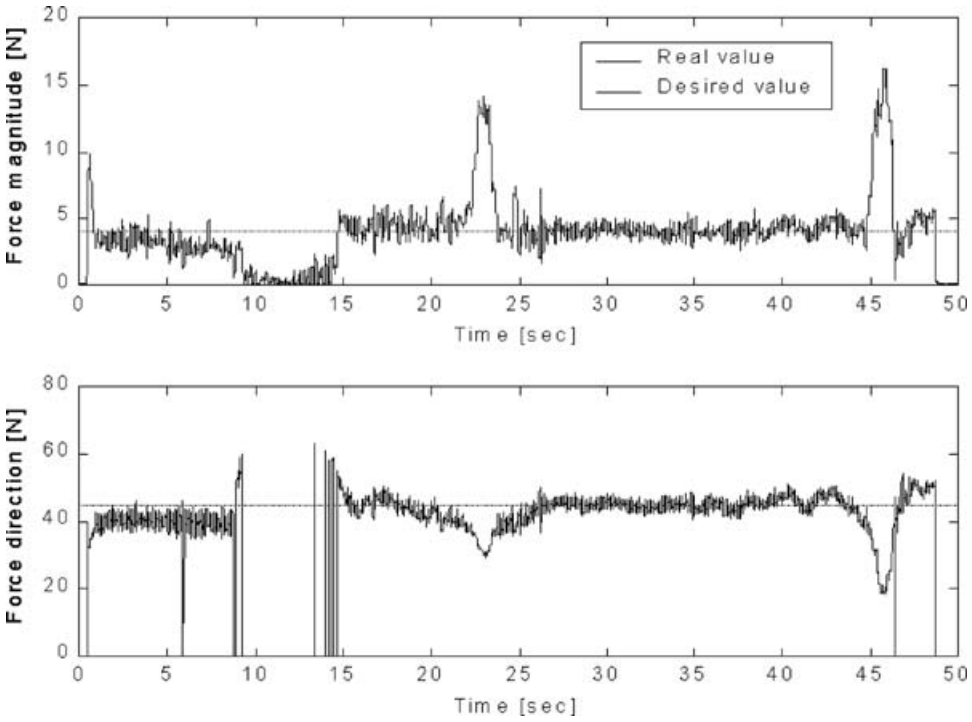


Fig. 11. Tracking result of a whole contour.

https://doi.org/10.1017/S0263574706003092 Published online by Cambridge University Press

References

1. J. Borenstein, "Experimental evaluation of a fiber optic gyroscope for improving dead-reckoning accuracy in mobile robots," *Proceedings of the IEEE Conference on Robotics and Automation* (1998) pp. 3456–3461.
2. L. Jetto, S. Longhi and G. Venturini, "Development and experimental validation of an adaptive extended Kalman filter for the localization of mobile robots," *IEEE Trans. Robot. Autom.* **15**(2), 219–229 (Apr. 1999).
3. T. D. Larsen, K. L. Hansen, N. A. Anderson and O. Ravn, "Design of Kalman filters for mobile robots; evaluation of the kinematics and odometric approach," *Proceedings of the IEEE Conference on Control Applications*, Piscataway, NJ (1999) pp. 1021–1026.
4. C. C. Tsai, "A localization system of a mobile robot by fusing dead-reckoning and ultrasonic measurements," *Proceedings of the IEEE Conference on Instrumentation and Measurement Technology*, Minnesota (May 18–21, 1998) pp. 144–149.
5. P. S. Jang, E. S. Jang, S. W. Jeon and S. Jung, "Neural network based guidance control of a mobile robot," *Proceedings of the International Conference on Control, Automations and Systems* (2003) pp. 1099–1104.
6. N. Sarkar, X. Yun, and V. Kumar, "Control of mechanical systems with rolling constraints: Application to dynamic control of mobile robots," *Int. J. Robot. Res.* **31**, 55–69 (1994).
7. I. Komanovsky and N. H. McClamroch, "Developments in non-hononomic control problems," *IEEE Control Syst. Mag.* **15**(6), 20–36 (1995).
8. Z. P. Jang and H. Nijmeijer, "Tracking control of mobile robots: A case study in backstepping," *Automatica* **33**(7), 1393–1399 (1997).
9. W. Wu, H. Chen and Y. Wang, "Backstepping design for path tracking of mobile robots," *Proceedings of the 1999 IEEE /RSJ International Conference on Intelligent Robots and Systems* (1999) pp. 1822–1827.
10. Y. Kanayama, Y. Kimura, F. Miyazaki and T. Noguchi, "A stable tracking control method for a non-holonomic mobile robot," *Proceedings of the IEEE /RSJ International Workshop on Intelligent Robots and Systems, IROS* (1991) pp. 1236–1241.
11. Y. Kanayama and F. Fahroo, "A new line tracking method for non-holonomic vehicles," *Proceedings of the IEEE Conference on Robotics and Automations* (1997) pp. 2908–2913.
12. Y. Chung, C. Park and F. Harashima, "A position control differential drive wheeled mobile robot," *IEEE Trans. Ind. Electron.* **48**(4), 853–863 (2001).
13. N. Hogan, "Impedance control: An approach to manipulator, part i, ii, iii," *ASME J. Dyn. Syst. Meas. Control* **3**, 1–24 (1985).
14. M. Raibert and J. Craig, "Hybrid position/force control of manipulators," *ASME J. Dyn. Syst. Meas. Control* **102**, 126–133 (1981).
15. R. Anderson and M. W. Spong, "Hybrid impedance control of robotic manipulators," *Proceedings of the IEEE Conference on Robotics and Automation* (1987) pp. 1073–1080.
16. G. J. Liu and A. A. Goldenberg, "Robust hybrid impedance control of robot manipulators," *Proceedings of the IEEE Conference on Robotics and Automation* (1991) pp. 287–292.
17. R. Colbaugh, H. Seraji and K. Glass, "Direct adaptive impedance control of robot manipulators," *J. Robot. Syst.* **10**, 217–248 (1993).
18. S. Jung and T. C. Hsia, "Robust neural force control scheme under uncertainties in robot dynamics and unknown environment," *IEEE Trans. Ind. Electron.* **47**(2), 403–412 (2000).
19. R. H. Byrne, C. T. Abdallah, and P. Dorato, "Experimental results in robust lateral control of highway vehicles," *IEEE Control Syst. Mag.* 70–76 (1997).
20. H. Fritz, "Longitudinal and lateral control of heavy duty trucks for automated vehicle following in mixed traffic: Experimental results from the CHAUFFEUR project," *Proceedings of the IEEE Conference on Control Applications* (1999) pp. 1348–1352.
21. L. Cai, A. B. Rad and K. Y. Cai, "A robust fuzzy PD controller for automatic steering control of autonomous vehicles," *Proceedings of the IEEE Conference on Fuzzy Systems* (2003) pp. 549–554.

https://doi.org/10.1017/S0263574706003092 Published online by Cambridge University Press